1   **Kif17 phosphorylation regulates its ciliary localization and photoreceptor outer segment**

2   **turnover**

3

4   Tylor R. Lewis[a,d], Sean R. Kundinger[b], Brian A. Link[a], Christine Insinna[a,c], and Joseph C.

5   Besharse[a,b*]

6

7   [a]*Department of Cell Biology, Neurobiology, and Anatomy*

8   *Medical College of Wisconsin, Milwaukee, WI, USA*

9

10   [b]*Department of Ophthalmology and Visual Sciences*

11   *Medical College of Wisconsin, Milwaukee, WI, USA*

12

13   [c]*Laboratory of Cell and Developmental Signaling*

14   *National Cancer Institute-Frederick, Frederick, MD, USA*

15

16   *Corresponding author

17   jbeshars@mcw.edu (JCB)

18

19   Other emails:

20

21   tylor.lewis@duke.edu (TRL)

22   sean.kundinger@emory.edu (SRK)

23   blink@mcw.edu (BAL)

24   christine.kettenhofen@nih.gov (CI)

25

26   Running Title: Kif17 and outer segment turnover

27

28   **Current addresses of TRL:**

29   [d]Department of Ophthalmology, Albert Eye Research Institute, Durham, NC 27710, USA

30

31

32

33

34

35

36

37   **Abstract**

38   **Background:** KIF17, a kinesin-2 motor that functions in intraflagellar transport, can regulate the

39   onset of photoreceptor outer segment development. However, the function of KIF17 in a mature

40   photoreceptor remains unclear. Additionally, the ciliary localization of KIF17 is regulated by a C-

41   terminal consensus sequence (KRKK) that is immediately adjacent to a conserved residue

42   (mouse S1029/zebrafish S815) previously shown to be phosphorylated by CaMKII. Yet, whether

43   this phosphorylation can regulate the localization, and thus function, of KIF17 in ciliary

44   photoreceptors remains unknown.

45   **Results:** Using transgenic expression in both mammalian cells and zebrafish photoreceptors, we

46   show that phospho-mimetic KIF17 has enhanced localization to cilia. Importantly, expression of

47   phospho-mimetic KIF17 is associated with greatly enhanced turnover of the photoreceptor outer

48   segment through disc shedding in a cell-autonomous manner, while genetic mutants of *kif17* in

49   zebrafish and mice have diminished disc shedding. Lastly, cone expression of constitutively

50   active tCaMKII leads to a *kif17*-dependent increase in disc shedding.

51   **Conclusions:** Taken together, our data support a model in which phosphorylation of KIF17

52   promotes its ciliary localization. In cone photoreceptor outer segments, this promotes disc

53   shedding, a process essential for photoreceptor maintenance and homeostasis. While disc

54   shedding has been predominantly studied in the context of the mechanisms underlying

55   phagocytosis of outer segments by the retinal pigment epithelium, this work implicates

56   photoreceptor-derived signaling in the underlying mechanisms of disc shedding.

57

60

Background

Cilia, organelles that project from the cell body and contain a microtubule-based axoneme, have numerous roles in development, signal transduction, and cell motility [1] and have garnered widespread interest due to associations with a widespread set of disorders termed ciliopathies [2]. Although the ciliary membrane is continuous with the plasma membrane, the transition zone at the base of the cilium is believed to function as a ciliary gate involved in regulating protein entry and exit [3]. While there has been conflicting evidence regarding the permeability barrier at the base of cilia [4, 5], it has been shown that ciliary entry of the kinesin-2 family member, KIF17, is dependent on a putative nuclear localization signal (NLS) **(Figure 1A)** that can additionally function as a ciliary localization signal (CLS) [6, 7]. Although KIF17 has been predominantly studied as a ciliary or dendritic motor [8], it has been reported to localize to the nucleus and function in transcriptional regulation [9, 10]. Yet the context under which a single conserved sequence can function as either a NLS or CLS remains unclear. Calcium/calmodulin-dependent protein kinase II, or CaMKII, has been shown to phosphorylate the C-terminus of KIF17 to regulate binding and release of Mint1, a scaffolding protein for motor cargo, in neurons [11]. Interestingly, this conserved phosphorylation site lies immediately adjacent to the NLS/CLS in KIF17 **(Figure 1A)**.

KIF17 is expressed in photoreceptors [12], which have a modified primary cilium called the outer segment (OS) that contains the components required for phototransduction [13]. Although KIF17 may regulate the onset of OS morphogenesis [14], there has been no evidence of a role for KIF17 in a mature photoreceptor [15]. As KIF17 can accumulate at the ciliary tip of photoreceptors [16], like mammalian cell lines [6, 7, 15, 17], it is possible that KIF17 may have some role in distal tip maintenance. Interestingly, the distal tip of the OS is phagocytized by the opposing retinal pigment epithelium (RPE) daily in a process called disc shedding [18]. The molecular mechanisms underlying disc shedding have been predominantly studied at the level of the RPE, but exposed phosphatidylserine (PS) on the tips of OS precedes disc shedding [19], suggesting photoreceptor signaling contributes to the underlying mechanism of disc shedding.

87   In this work, we express three different forms of mCherry-tagged mouse KIF17 (wild-type,

88   phospho-mimetic S1029D, and phospho-deficient S1029A) **(Figure 1B)** in four separate

89   mammalian cell lines and show that phospho-mimetic KIF17(S1029D) accumulates extensively in

90   cilia compared to either wild-type KIF17 or phospho-deficient KIF17(S1029A). Significant

91   differences in nuclear localization of the transgenes were only seen in two of four cell lines, where

92   KIF17(S1029D) had restricted nuclear localization. Additionally, with cone expression of three

93   different forms of GFP-tagged zebrafish Kif17 (wild-type, phospho-mimetic S815D, and phospho-

94   deficient S815A) **(Figure 1C)**, we show that the accumulation of Kif17 in the zebrafish OS is

95   controlled through this phosphorylation site. Cone expression of phospho-mimetic Kif17 leads to a

96   three-fold increase in disc shedding, while the genetic mutant *kif17*^{mw405} has diminished disc

97   shedding. Additionally, cone expression of a constitutively active CaMKII leads to a two-fold

98   increase in disc shedding in wild-type, but not *kif17*^{mw405} mutant fish. Taken together, this work

99   supports a model in which phosphorylation of Kif17 regulates its accumulation in cilia. In cone

100   photoreceptors, phosphorylated Kif17 in the OS participates in a cell-autonomous process to

101   promote disc shedding.

102

103   **Results**

104   **Phospho-mimetic mouse KIF17 has enhanced ciliary localization**

105   Published data suggest that the conserved KRKK sequence in the C-terminus of KIF17

106   can function as both a NLS and CLS [6]. Interestingly, a conserved phosphorylation site (S1029 in

107   mice and S815 in zebrafish) lies immediately adjacent to this NLS/CLS **(Figure 1A)** and has been

108   shown to be phosphorylated by CaMKII in neurons [11]. To further investigate this phosphorylation

109   site with regards to ciliary and nuclear localization, we generated three different constructs of

110   mouse KIF17 for mammalian cell expression with the CMV promoter: KIF17-mCherry, phospho-

111   mimetic KIF17(S1029D)-mCherry, and phospho-deficient KIF17(S1029A)-mCherry **(Figure 1B)**.

112   To investigate the extent to which this phosphorylation site controls ciliary and nuclear localization,

113   we used four different ciliated mammalian cell lines: LLC-PK1, a pig kidney epithelial line; HEK-

114   293, a human kidney line; hTERT-RPE1, a human retinal pigment epithelial line; and IMCD3, a

115   mouse kidney line. With transient transfection of serum-starved cells, we can determine the extent

116   of ciliary localization of each transgene with co-labeling of acetylated α-tubulin, which labels the

117   axoneme, or nuclear localization with co-labeling of Hoechst **(Figure 2A)**. The frequency of ciliary

118   localization of the phospho-mimetic KIF17(S1029D)-mCherry was significantly increased between

119   two- to four-fold over the phospho-deficient KIF17(S1029A)-mCherry in all cell lines studied

120   **(Figure 2B)**. Interestingly, the ciliary localization of wild-type KIF17-mCherry was never

121   significantly different from the phospho-deficient KIF17(S1029A)-mCherry with both having a

122   baseline level of ciliary localization, suggesting that phosphorylation enhances ciliary localization

123   but does not absolutely control ciliary entry.

124   To analyze nuclear localization, we calculated the ratio of average mCherry signal intensity

125   between the nucleus and cytoplasm **(Figure S1)**. In two of the four cell lines (LLC-PK1 and HEK-

126   293), there were no effects on transgene localization between the nucleus and cytoplasm despite

127   there being a ciliary localization difference. However, in hTERT-RPE1 and IMCD3 cells, the

128   phospho-mimetic KIF17(S1029D)-mCherry had a decreased nuclear to cytoplasmic ratio,

129   suggesting inhibition of nuclear localization as compared to either wild-type KIF17-mCherry or

130   phospho-deficient KIF17(S1029A)-mCherry. Yet, only in hTERT-RPE1 cells did the nuclear to

131   cytoplasmic ratio exceed one. Taken together, these data support a model in which

132   phosphorylation of the conserved S1029 residue of mouse KIF17 strongly promotes ciliary

133   localization in four different cell lines. In contrast, nuclear localization of KIF17 may be negatively

134   regulated by phosphorylation depending on cell type.

135

136   **Phospho-mimetic zebrafish Kif17 has enhanced OS localization**

137   While phosphorylation of KIF17 may regulate ciliary localization in mammalian cells, our

138   main interest was in investigating the effect of KIF17 phosphorylation in ciliary photoreceptor OS

5

139   *in vivo*. We generated comparable zebrafish Kif17 constructs specifically for cone photoreceptor

140   expression with the cone-specific transducin-α (*gnat2*) promoter, also known as TaCP: Kif17-GFP,

141   phospho-mimetic Kif17(S815D)-GFP, and phospho-deficient Kif17(S815A)-GFP **(Figure 1C)**.

142   While previous work shows that Kif17-GFP can accumulate at the distal tip of the OS [16], we used

143   transient injections of each of these constructs into wild-type zebrafish embryos to quantify

144   localization within the OS of two sub-types of zebrafish cones: blue and green absorbing cones.

145   Supporting the mammalian cell work, phospho-mimetic Kif17(S815D)-GFP accumulated in the OS,

146   while phospho-deficient Kif17(S815A)-GFP appeared to accumulate at the base of the OS

147   **(Figures 3A, S2)**. The accumulation of phospho-mimetic Kif17(S815D)-GFP in the OS was seven-

148   fold greater than that of phospho-deficient Kif17(S815A)-GFP **(Figure 3B)**. Additionally, line

149   intensity analysis reveals that phopsho-mimetic Kif17(S815D)-GFP localizes evenly along the

150   entire length of the OS, while phospho-deficient Kif17(S815A)-GFP exhibited a specific

151   accumulation at the base of the OS **(Figure 3C)**. We did not observe any evidence of nuclear

152   localization of the zebrafish Kif17-GFP constructs **(Figure S2)**. These data further support a model

153   in which phosphorylation of Kif17 leads to an enhanced localization in the ciliary photoreceptor

154   OS.

155

156   **KIF17 promotes cell-autonomous disc shedding**

157   While we have previously shown a developmental role of KIF17 in regulating the onset of

158   OS morphogenesis [14], there is no evidence of a role of KIF17 in mature photoreceptors [15]. We

159   hypothesized that investigating the temporal expression patterns of *Kif17* in mature photoreceptors

160   throughout the diurnal light:dark cycle could shed light on a potential function of KIF17. We

161   performed qPCR on mouse retinas that were collected every four hours during a 24 hour period

162   beginning at light onset, indicated as Zeitgeber Time (ZT) 0, through dark onset (ZT 12), and

163   stopping at ZT 20, or 20 hours following light onset. Interestingly, there is a single peak in *Kif17*

164   expression in the mouse retina at ZT 4, just following light onset, which subsequently returns to a

6

165   basal level **(Figure S3A)**. We also performed qPCR on 14 dpf zebrafish eyes that were collected

166   at nine discrete timepoints over a 24 hour period beginning at light onset. In contrast to the mice,

167   which are kept on a 12 hour:12 hour light:dark cycle, the zebrafish are maintained on a 14 hour:10

168   hour light:dark cycle, so that ZT 14 indicates dark onset. While there is an increase in zebrafish

169   *kif17* expression immediately after light onset (ZT 1.5), there is a second, more intense peak just

170   following dark onset (ZT 16 and ZT 18) **(Figure S3B)**. While *Kif17* appears to be rhythmically

171   expressed in both mouse and zebrafish, mice have a single peak of expression associated with

172   light onset, whereas zebrafish have two peaks of expression associated with both light and dark

173   onset.

174   Due to the association of *kif17* expression with both light and dark onset in zebrafish, we

175   hypothesized that Kif17 could be involved in disc shedding, the daily process of OS turnover in

176   which RPE cells adjacent to the OS phagocytize and degrade shed OS tips. To analyze disc

177   shedding, we performed transmission electron microscopy (TEM) on 5dpf zebrafish larvae that

178   had been injected with the cone-expressing plasmids encoding either one of the three Kif17

179   transgenes or a soluble GFP control. Lacking transposase, the plasmids do not incorporate into

180   the genome but rather facilitate episomal expression of transgenes. Interestingly, transient

181   expression of the phospho-mimetic Kif17(S815D)-GFP was sufficient to drive an increase in the

182   number of phagosomes compared to wild-type Kif17, phospho-deficient Kif17, or the soluble GFP

183   control **(Figure S4)**. Because of the potential for interactions of the Kif17 transgenes with

184   endogenous wild-type Kif17 and the transient and mosaic nature of expression of injected

185   plasmids, we generated stable lines of each of our cone-expressing transgenes (Kif17-GFP,

186   phospho-mimetic Kif17(S815D)-GFP, and phospho-deficient Kif17(S815A)-GFP) on a mutant

187   background called *kif17[mw405]* lacking endogenous Kif17 [14]. Following several generations of out-

188   crossing to ensure only a single copy was inserted for each transgene **(Figure S5A,B)**, we

189   collected 7dpf larvae with comparable levels of expression **(Figure S5A,C)** at ZT 1.5 and

190   performed TEM to analyze phagosomes **(Figure 4A)**. There was a dramatic three-fold increase in

7

191   the number of phagosomes observed in the RPE in retinas with cone expression of Kif17(S815D)-

192   GFP as compared to either Kif17-GFP or Kif17(S815A)-GFP **(Figure 4B)**, while the average size

193   of phagosomes was unchanged **(Figure 4C)**. Surprisingly, while there was a significant increase

194   in disc shedding associated with Kif17(S815D)-GFP expression in cones, there was no decrease

195   in average OS area **(Figure 4D)**, suggesting that the excess in disc shedding may compensate for

196   excess OS morphogenesis. However, an upregulation of opsin mRNA expression, which encodes

197   the major protein of the OS, was not observed **(Figure S6)**.

198   Because our TEM analysis does not distinguish between phagosomes from either cone or

199   rod photoreceptors, we performed immunogold labeling of these transgenic larvae. Using a

200   monoclonal antibody against bovine rhodopsin, K62-171c [20], that also specifically labels

201   zebrafish rhodopsin-containing OS and phagosomes **(Figures 4E, S7)**, we show that cone

202   expression of Kif17(S815D)-GFP leads to a three-fold increase in unlabeled phagosomes,

203   presumably from cones, compared to larvae with cone expression of Kif17(S815A)-GFP **(Figure**

204   **4F)**. However, there is no significant change in the number of rhodopsin-labeled phagosomes.

205   Additionally, we specifically labeled cone-derived phagosomes using an antibody against gnat2,

206   the cone-specific transducin-α whose promoter was used to drive expression of the transgenes in

207   this study. Although the immunogold labeling of cone transducin-α labeled both cone OS and

208   phagosomes **(Figure S8A)**, the labeling efficiency was significantly lower than that of the rhodopsin

209   antibody, presumably due to a lower concentration of gnat2 in the OS. Nonetheless, we show that

210   cone expression of Kif17(S815D)-GFP leads to a two-fold increase in cone transducin-α-labeled

211   phagosomes with no significant change in unlabeled phagosomes, presumably from rods **(Figure**

212   **S8B)**. Taken together, these data suggest phosphorylation of Kif17 promotes both OS localization

213   and subsequent cone disc shedding in a cell-autonomous manner.

214

215   **Loss of KIF17 diminishes disc shedding in zebrafish and mice**

216   While transgenic cone expression of phospho-mimetic Kif17(S815D)-GFP promotes disc

217   shedding, we sought to further investigate how the loss of *kif17* affects disc shedding. While we

218   did not observe defects in disc shedding in *kif17^{mw405}* mutants at the single timepoint (ZT 1.5)

219   analyzed in our experiments with the transgenic fish **(Figure 4B)**, we proposed that deficiencies

220   of disc shedding in the *kif17^{mw405}* zebrafish would be better observed when analyzed throughout

221   the entire day. We collected larvae at 14 dpf, when OS have reached their mature size [14], at the

222   nine timepoints over a 24 hour period and performed TEM to image phagosomes in both wild-type

223   and *kif17^{mw405}* zebrafish. We find that zebrafish disc shedding is highly rhythmic, with two peaks

224   associated with both light and dark onset. Additionally, there is a significant decrease in the number

225   of phagosomes shed in zebrafish lacking Kif17 (*kif17^{mw405}*) as compared to controls **(Figure 5A)**.

226   Although there were changes in the disc shedding rates between genotypes and throughout the

227   day, there was no change in phagosome size **(Figure 5B)**.

228   To more carefully analyze the differences in disc shedding patterns between wild-type and

229   *kif17^{mw405}* larvae as well as between the morning and evening peaks, we performed spline

230   interpolation, a method of constructing a piecewise polynomial curve to smoothly fit the disc

231   shedding data across all timepoints, for both the wild-type and *kif17^{mw405}* phagosome number data

232   **(Figure S9A)**. For wild-type larvae, the two peaks in the number of phagosomes occurred 2.5

233   hours after light onset and subsequently 2 hours after dark onset **(Table S1)**. In comparison,

234   *kif17^{mw405}* mutants had estimated peaks at 2.5 hours after light onset, and 3.2 hours after dark

235   onset, suggesting that, in addition to the decrease in the total number of phagosomes shed

236   associated with loss of *kif17*, the kinetics of disc shedding at night might also be altered.

237   Additionally, the kinetics of phagosome digestion could be roughly estimated by the decreasing

238   slope in the number of phagosomes observed following either the morning or night peak. However,

239   this is under the assumption that there are no new phagosomes being shed during this period.

240   Following the morning peak of disc shedding, we estimated similar slopes of 8×10^{-3} and 10×10^{-3}

241   phagosomes/μm of RPE per hour in wild-type and *kif17^{mw405}* larvae respectively. Again, after the

242   evening peak we estimated similar slopes of 9×10^{-3} and 8×10^{-3} phagosomes/μm of RPE per hour

243   for wild-type and *kif17*^{*mw405*} larvae respectively. Taken together, these data suggest that the half-

244   life of a phagosome of approximately 3-4 hours is unaffected by the loss of *kif17*.

245   In addition to the deficiencies in disc shedding caused by loss of *kif17* in zebrafish, we

246   observed a similar diminution in total number of phagosomes in *Kif17* deficient mice **(Figure 5D)**

247   without a significant impact on phagosome size **(Figure 5E)**. In contrast to the report that rat disc

248   shedding occurs in only a single peak following light onset [21], we observed two peaks of disc

249   shedding in mice, more comparable to our findings in zebrafish: one shortly after light onset and

250   another shortly after dark onset. We further performed spline interpolation on both the wild-type

251   and *Kif17*^{*tm1b(Bjc)*} phagosome number data **(Figure S9B)** and estimated that the morning peak in

252   phagosome number occurred 1.4 hours after light onset in wild-type compared to 0.7 hours in

253   *Kif17*^{*tm1b(Bjc)*} mice, while the evening peak was estimated to occur at about 1.7 hours after dark

254   onset for both genotypes **(Table S2)**. Following the morning peak of disc shedding, phagosome

255   number decreased at similar rates of 9×10^{-3} and 11×10^{-3} phagosomes/μm of RPE per hour in wild-

256   type mice compared *Kif17*^{*tm1b(Bjc)*} mice. After the evening peak, the number of phagosomes

257   decreased at similar rates of 6×10^{-3} and 7×10^{-3} phagosomes/μm of RPE per hour in wild-type and

258   *Kif17*^{*tm1b(Bjc)*} mice respectively. Under all conditions, the half-life of a phagosome in mice is

259   approximately 1-2 hours. As in zebrafish, this analysis suggests little if any alteration in the kinetics

260   of phagosome accumulation or digestion from loss of *Kif17*. In both mice and zebrafish, loss of

261   *Kif17* is associated with a decrease in the total number of phagosomes, supporting a role for KIF17

262   in promoting disc shedding in the mature photoreceptor.

263   It has been suggested in an analysis using goldfish [22] that morning and evening peaks

264   reflect disc shedding by rods and cones respectively, although the two types of phagosomes

265   cannot be readily distinguished after phagocytosis. To further define these two peaks of disc

266   shedding in zebrafish, we performed the immunogold rhodopsin labeling of phagosomes in wild-

267   type larvae at both the morning (ZT 1.5) and evening (ZT 15.5) peaks. While there was no change

10

268   in the total number of phagosomes at either of these peaks, there was an increase in the number

269   of unlabeled phagosomes at the evening peak, suggesting an increase in cone disc shedding

270   **(Figure 5C)**. However, at least 25% of the phagosomes present at the night peak were still rod

271   phagosomes. Additionally, we performed immunogold labeling with the cone-specific transducin-

272   α antibody, and again found that while there was no change in the total number of phagosomes at

273   either the morning or evening peak, the evening peak contains a higher ratio of cone to rod

274   phagosomes than the morning peak **(Figure S8C)**. However, cone phagosomes still composed

275   about 40% of the phagosomes in the morning peak, while unlabeled phagosomes compose about

276   40% of the evening peak. Overall, there are two peaks of phagosomes in zebrafish: one shortly

277   after light onset with a slightly higher proportion of rod phagosomes and another peak occurring

278   shortly after dark onset with a slightly higher proportion of cone phagosomes. These zebrafish data

279   ultimately do not support the absolute distribution of cone shedding at night and rod shedding

280   during the day as is commonly reported in the literature [22], but rather only a small bias of cone

281   shedding at night and rod shedding during day. Additionally, we performed immunogold rhodopsin

282   labeling of phagosomes in mice with B630, a mouse monoclonal anti-rhodopsin, at both the

283   morning (ZT 1.5) and evening (ZT 13.5) peaks. At both peaks, the majority of phagosomes

284   contained rhodopsin, although there was a small proportion of unlabeled phagosomes presumably

285   from cones **(Figure 5F)**. Of note, there was no significant increase in the number of these

286   unlabeled phagosomes at the night-time peak.

287

288   **Constitutively active CaMKII promotes disc shedding in a Kif17 dependent manner**

289   While we have shown that amino acid changes at the conserved zebrafish S815

290   phosphorylation site can control KIF17 localization and promote photoreceptor disc shedding, we

291   sought to associate this regulation more directly to CaMKII, which phosphorylates this conserved

292   serine of KIF17 in neurons [11] and is expressed in cones [23]. We injected tCaMKII-GFP, a

293   constitutively active form of CaMKII [24], under control of the TaCP cone promoter and investigated

11

294   disc shedding at 7dpf as compared to control larvae injected with soluble GFP under control of the

295   same cone promoter. We found that wild-type larvae injected with tCaMKII-GFP had a two-fold

296   increase in phagosome number as compared to soluble GFP controls. However, this increase in

297   disc shedding did not occur when tCaMKII-GFP was injected in *kif17^{mw405}* larvae **(Figure 6A)**.

298   There was no change in phagosome size associated with any of the injected larvae **(Figure 6B)**.

299   Ultimately, these data show that the effect of tCaMKII depends on the presence of endogenous

300   Kif17 and implicates CaMKII mediated phosphorylation of Kif17 in the regulation of disc shedding.

301

302   **Discussion**

303   **Phosphorylation promotes ciliary localization of KIF17**

304   In this work, we show that phospho-mimetic KIF17 has a strongly enhanced ciliary

305   localization in four different mammalian cell lines and in zebrafish photoreceptors. We propose two

306   distinct models for the regulation of ciliary localization of KIF17 via phosphorylation **(Figure 7)**. In

307   the first model, phosphorylation of KIF17 via CaMKII could promote the ciliary entry of KIF17.

308   However, because both wild-type and phospho-deficient KIF17 have a basal level of ciliary

309   localization, ciliary entry of non-phosphorylated KIF17 does not appear to be entirely restricted. In

310   a second model, phosphorylation could promote accumulation within the OS, potentially at the

311   distal tip as has been shown previously [6, 7, 15-17], through an interaction with a plus-end

312   microtubule associated protein. KIF17 has a consensus sequence for EB1-binding and

313   microtubule plus-end accumulation [25] and has been shown to interact with EB1 in epithelial cells

314   for regulating microtubule dynamics at the plus-ends of cytoplasmic microtubules [26]. EB1 also

315   localizes to the axonemal tip of flagella in *Chlamydomonas reinhardtii* [27]. Thus, enhanced affinity

316   for EB1 (or another related microtubule associated protein) via phosphorylation of KIF17 could

317   lead to the increased ciliary localization. De-phosphorylation could subsequently release KIF17

318   from this interaction, leading to removal from the cilia via either active transport or diffusion. In

319   support of this model, truncated KIF17 lacking the motor domain is still able to accumulate at the

320   ciliary tip [7, 15, 17], implying the need for some additional microtubule-associated protein for

321   KIF17 ciliary localization.

322   In contrast to the strong promotion of ciliary localization, there was only a mild, cell line-

323   dependent restriction of nuclear localization associated with phospho-mimetic KIF17. There are

324   two explanations for these data: that KIF17 phosphorylation can directly inhibit nuclear entry only

325   in certain cellular contexts or that the mild effects on nuclear entry are secondary effects of the

326   strong promotion of ciliary localization. However, because all four cell lines depict a strong

327   promotion of ciliary localization of phospho-mimetic KIF17, it is unlikely that the effects on nuclear

328   localization seen in only two of the cell lines are secondary effects. Ultimately, this evidence

329   suggests that KIF17 phosphorylation is a robust regulator of ciliary localization in a variety of cell

330   types, including photoreceptors, and in a variety of species, with much milder effects on nuclear

331   localization.

332

333   **KIF17 positively regulates disc shedding**

334   The function of Kif17 in zebrafish photoreceptors has been ambiguous. While early

335   morpholino knockdown experiments suggested that Kif17 was important for OS development [12],

336   two genetic mutants [28, 29] were shown to have morphologically normal OS. Similarly, mice were

337   shown to have morphologically normal photoreceptors [15]. We recently resolved these apparent

338   contradictions by showing that loss of Kif17 delays the onset of OS morphogenesis in both

339   zebrafish and mice [14]. Nonetheless, OS in both species attain normal morphology and

340   dimensions [14, 15], raising the question of whether Kif17 functions in a mature photoreceptor.

341   In this work, we find significant decreases in disc shedding in both $kif17^{mw405}$ zebrafish and

342    $Kif17^{tm1b(Bjc)}$ mice. While disc shedding is not completely ablated with loss of $Kif17$, we have

343   previously proposed that additional factors, such as kinesin-II or diffusion, can compensate for

344   defects in trafficking in $Kif17$ mutant photoreceptors [14]. Whether other factors compensate for

345   loss of KIF17's function in promoting disc shedding and whether attenuating such factors can lead

                                                                                                          13

346   to compound effects in *Kif17* mutants on disc shedding remains to be elucidated. Additionally, cone

347   expression of transgenic phospho-mimetic Kif17 results in a cell-autonomous enhancement of disc

348   shedding. CaMKII appears to be one of the kinases responsible for phosphorylation of Kif17 in

349   photoreceptors *in vivo*, as cone expression of constitutively active tCaMKII promotes disc shedding

350   in a *kif17*-dependent manner. However, additional investigation is required to identify other

351   potential kinases or the phosphatase that may regulate removal of Kif17 from the OS. Ultimately,

352   the phospho-mimetic Kif17 "gain of function" effects in promoting disc shedding combined with

353   decreased disc shedding phenotype associated with genetic loss of Kif17 strongly implicate Kif17

354   in an important role regulating disc shedding at the level of the photoreceptor. Major advances

355   have been made regarding the regulation of disc shedding, but most of that work has been at the

356   level of phagocytosis by adjacent RPE cells [30-32]. However, PS exposure at the distal OS

357   precedes shedding events [19], and these data on Kif17 further imply an active process in the

358   ciliary OS tip that promotes detachment of the distal domain and subsequent phagocytosis.

359   Another significant conclusion from this work is that photoreceptors can exhibit

360   considerable plasticity in the kinetics of ciliary OS turnover while still maintaining normal

361   dimensions. It is well known that mouse rods shed approximately 10% of their length daily and

362   maintain a steady-state length through compensating OS renewal [33]. In the *Kif17* mutant mice

363   and zebrafish, diminished disc shedding is not accompanied by reduced size of the OS [14],

364   suggesting an overall slower rate of renewal at the OS base. Likewise, the dimensions of the OS

365   are unchanged in the "gain of function" experiments involving phospho-mimetic transgene

366   expression, implying that enhanced disc shedding is compensated for by enhanced OS formation.

367   While we propose that Kif17 is implicated in regulating disc shedding directly given this work, it is

368   possible that Kif17 is involved in promoting new morphogenesis at the OS base and the increased

369   disc shedding is a secondary effect to maintain a steady-state OS. Although the open disc

370   conformation of cone photoreceptors complicates experiments, techniques involving

371   autoradiography [34] and fluorescent [35] pulse-labels to study the dynamics of rod OS

372   morphogenesis can be applied to investigate the changes in rates of new cone OS morphogenesis

373   associated with either gain or loss of function of Kif17.

374   As little is known about the photoreceptor-derived signaling that regulates disc shedding,

375   the specific mechanism by which Kif17 promotes disc shedding is unclear. However, as PS

376   exposure at the distal OS precedes disc shedding [19], it is possible that Kif17 is involved in

377   regulating the localization of a putative scramblase [36] or floppase [37] involved in mediating PS

378   transport from the cytosolic to extracellular leaflet of the OS membrane. Alternatively, Kif17

379   accumulated at the distal OS could interact with various ligands expressed in the photoreceptor,

380   such as SEMA4D, that are involved in regulating disc shedding via receptors in the RPE [38].

381   Future work will address potential interacting partners of Kif17 to reveal how accumulation at the

382   distal OS promotes disc shedding.

383

384   **Temporal regulation of cone and rod disc shedding**

385   Our investigation of Kif17 loss of function required analysis of disc shedding at multiple

386   timepoints because photoreceptor turnover is well-known to occur on a diurnal schedule [21, 22,

387   39], which led to unexpected surprises in our analysis in both zebrafish and mice. First, it is

388   generally thought that rods shed in the morning after light onset, while cones do so in the evening

389   after dark onset [22, 40, 41]. However, this has been generally determined by counting

390   phagosomes in the RPE where the differences between the two cell types are not apparent. Our

391   new data using immunogold labeling specific for either rods (using the rhodopsin antibody) or

392   cones (using the GNAT2 antibody) shows that both rod and cone phagosomes are present at both

393   day-time and night-time peaks in zebrafish. Our interpretation of these data is that both rods and

394   cones shed discs at either time of day, although there is a slight preponderance of rod phagosomes

395   in the morning and cones at night. At the very least, the absolute idea of "rods shed during the day

396   and cones at night" [22] must be reconsidered. Secondly, we observed equal peaks of disc

397   shedding in mice both after light onset and offset, which contrasts with the long-held view that disc

398   shedding in rod-dominated rodents occurs principally after light onset [21]. This can hardly be

399   explained as a dichotomy of rod versus cone shedding as the mouse retina consists of ~97% rods

400   and ~3% cones [42]. A key difference in our analysis in mice is that we sampled at symmetric time

401   points, including both 1.5 hours after both light onset and dark onset, whereas other studies have

402   used wider sampling intervals such as 4 hour intervals, possibly missing important events occurring

403   after dark onset [21]. This surprising finding is of potential broad significance in understanding disc

404   shedding and OS turnover and is under current investigation.

405

406   **Conclusion**

407   Overall, we show that phosphorylation of KIF17 promotes its ciliary localization. In cone

408   photoreceptor outer segments, phosphorylated KIF17 promotes cell-autonomous disc shedding.

409   As disc shedding has been predominantly studied within the retinal pigment epithelium, this work

410   implicates photoreceptor-derived signaling in the underlying mechanisms of disc shedding.

411

412   **Methods**

413   **Mouse and zebrafish husbandry**

414   C57BL/6 mice were maintained under 12 hour:12 hour light:dark cycle. We generated the

415   *Kif17*$^{tm1b(Bjc)}$ mouse line as described previously [14]. Adult ZDR zebrafish were housed at 28.5°C

416   on a 14 hour:10 hour light:dark cycle. Embryos were raised at 28.5°C on a 14 hour:10 hour

417   light:dark cycle. We generated the *kif17*^{mw405} zebrafish line as described previously [14]. All

418   experiments were approved and conducted in accordance with the Institutional Animal Care and

419   Use Committee of the Medical College of Wisconsin. For all experiments involving animals, a

420   biological replicate is defined as a single mouse or single zebrafish. Male and female animals were

421   randomly assigned to each experimental group. For both zebrafish and mice, littermate animals

422   were used.

423

Cloning of constructs

A plasmid encoding CMV:KIF17-mCherry was generated as previously reported [16]. Overlap extension PCR was performed to create the two mouse phospho-mutants: CMV:KIF17(S1029D)-mCherry and CMV:KIF17(S1029A)-mCherry. The wild-type codon sequence for S1029, AGC, was mutated to GAC for S1029D and GCC for S1029A. A plasmid encoding TaCP:Kif17-GFP was generated as previously reported [16]. Overlap extension PCR was performed to create the two zebrafish phospho-mutants: TaCP:Kif17(S815D)-GFP and TaCP:Kif17(S815A)-GFP. The wild-type codon sequence for S815, AGC, was mutated to GAC for S815D and GCC for S815A. The constitutively active CaMKII (tCaMKII-GFP) was generated by Yasunori Hayashi [24]. tCaMKII-GFP was cloned downstream of the TaCP promoter using the Gateway Cloning system (Invitrogen). The control TaCP:GFP plasmid was generated by Breandán Kennedy [43].

Zebrafish transgenesis

For various experiments involving injected larvae, 9.2nL of a working solution containing 25ng/µL of a plasmid (encoding either TaCP:Kif17-GFP, TaCP:Kif17(S815D)-GFP, TaCP:Kif17(S815A)-GFP, TaCP:tCaMKII-GFP, or TaCP:GFP), as well as 0.05% phenol red, were injected into ZDR embryos at the 1-cell stage. For stable line generation of TaCP:Kif17-GFP, TaCP:Kif17(S815D)-GFP, and TaCP:Kif17(S815A)-GFP, 10ng/µL transposase RNA was included in the injection solution to facilitate genome integration [44]. Injected embryos were subsequently raised and outcrossed to screen for germ-line transmission. GFP-positive embryos were raised and outcrossed for several generations to establish a stable line of low-expressing, single insert transgenic fish to minimize non-specific effects due to high levels of over-expression **(Figure S5A,B)**. For experiments, embryos were imaged with epifluorescence at 4dpf and fluorescence intensity of eyes was quantified to ensure an identical expression level between the three transgenes **(Figure S5A,C)**.

17

Antibodies

Commercial primary antibodies included: 6-11B-1, or mouse monoclonal anti-acetylated α-tubulin (Sigma), rabbit polyclonal anti-GNAT2 (MBL International). The rabbit polyclonal anti-green and blue cone opsin antibodies were gifts from Dr. Thomas Vihtelic (University of Notre Dame) [45]. The mouse monoclonal anti-rhodopsin antibodies K62-171c and B630 were gifts from Dr. Paul Hargrave (University of Florida) [20]. Nuclei were stained with Hoechst (Thermo Scientific). Fluorescent secondary antibodies included goat anti-mouse IgG Alexa Fluor 488 and goat anti-rabbit IgG Alexa Fluor 594. Immunogold labeling secondary was either goat anti-mouse IgG 10nm colloidal gold (Electron Microscopy Sciences) or goat anti-rabbit IgG 10nm colloidal gold (Electron Microscopy Sciences).

Mammalian cell culture analysis

LLC-PK1 (ATCC CL-101), HEK-293 (ATCC CRL-1573), hTERT-RPE1 (ATCC CRL-4000), and IMCD3 (ATCC CRL-2123) were obtained from ATCC. Cell line authentication and testing of mycoplasma-negative were performed by ATCC. Additional testing of mycoplasma infection is performed biannually with MycoAlert (Lonza). LLC-PK1 cells were grown in Medium 199 (Gibco), HEK-293 cells were grown in DMEM (Gibco), and hTERT-RPE1 and IMCD3 cells were grown in DMEM/F12 (1:1) (Gibco). All media were supplemented with 10% FBS and 1% penicillin and streptomycin and cells were grown at 37°C in 5% CO_2. For ciliogenesis and transfection, cells were transferred to Opti-MEM (Gibco) at 60-80% confluency and transiently transfected with Lipofectamine 3000 (Invitrogen). Serum-starvation in Opti-MEM induced ciliogenesis and after 24 hours, cells were fixed in 4% PFA for 20 minutes and subsequently immunostained with acetylated α-tubulin to indicate cilia and Hoechst to label nuclei. Because of the nature of transient transfection, there were a variety of transgenic expression levels. Approximately 20% of cells with a high level of expression in which transgene appeared to be highly vesicular or stuck in Golgi were excluded from analysis. For analysis, five separate transfections of each transgene in each

476   cell line were performed. For ciliary localization in each cell line, the number of cells with mCherry

477   labeling of the cilia was counted and divided by the total number of transfected cells. For nuclear

478   localization, ImageJ was used to quantify the average intensity of both cytoplasmic and nuclear

479   mCherry signal. Following subtraction of the average intensity of the background of each image

480   (quantified from an area where there was no cellular fluorescence), the ratio of the cytoplasmic to

481   nuclear average intensity was calculated.

482

483   **Photoreceptor localization analysis**

484   Embryos were injected with constructs as described above for mosaic expression and raised in

485   phenylthiourea (PTU) to delay melanin pigment formation. At 4 dpf, larvae were anesthetized with

486   tricaine and screened for GFP fluorescence. Immunofluorescence staining was performed on

487   cryosections of 5 dpf GFP-positive larvae as previously described [12] with antibodies to green or

488   blue opsin to label cone OS and Hoechst to label nuclei. For quantification, only injected larvae

489   with positive transgenic expression were analyzed. For OS localization, GFP labeling in the opsin-

490   labeled OS was analyzed compared to the total number of transgene-expressing cones. For line

491   intensity analysis, a line along the length of the OS (as determined by opsin-labeling) was used to

492   calculate GFP signal intensity in ImageJ. For standardization of levels of transgene expression, all

493   intensity values along a single line were standardized to the maximum value along that line.

494   Additionally, to standardize for variations in lengths of the OS, the length of an OS was split into

495   ten equal groups based on position from base to distal OS and intensity values were averaged for

496   each of these ten groups to generate data for a single technical replicate. In each biological

497   replicate, several technical replicates were averaged, as described in captions.

498

499   **Disc shedding analysis**

500   For transgenic or injected larva disc shedding analyses, zebrafish embryos were raised in

501   phenylthiourea until 4 dpf when they could be screened for GFP fluorescence. GFP-positive

19

502   embryos were then raised in regular fish water until either 5dpf **(Figure S4)** or 7dpf (rest of the

503   experiments), when they were collected at 1.5 hours following light onset. For zebrafish diurnal

504   disc shedding analysis, 14dpf wild-type and $kif17^{mw405}$ larvae were collected at nine different

505   timepoints following light onset: 0 (light onset), 1.5 hours, 3.5 hours, 7.5 hours, 10.5 hours, 14

506   hours (dark), 15.5 hours, 17.5 hours, 20.5 hours. Collected larvae were processed as previously

507   described for TEM [14]. For mouse diurnal disc shedding analysis, 2- to 4-month old C57BL/6 and

508    $Kif17^{tm1b(Bjc)}$ litter-mate mice were collected at eight different timepoints following light onset: 0 (light

509   onset), 1.5 hours, 4.0 hours, 8.0 hours, 12 hours (dark), 13.5 hours, 16 hours, and 20 hours. Mice

510   were euthanized and whole eyes were processed as previously described for TEM [14]. For

511   zebrafish analysis, five larvae were analyzed for each genotype and timepoint for a total of 45

512   larvae per genotype. For mouse analysis, three mice were analyzed for each genotype and

513   timepoint for a total of 24 mice per genotype. For phagosome number analysis, the number of

514   phagosomes was counted and divided by the total length of RPE measured. For phagosome size

515   analysis, phagosome area was measured and averaged for each sample. For OS size analysis,

516   OS area was measured and averaged for each sample.

517

518   **Spline interpolation analysis**

519   For zebrafish, cubic spline interpolation was performed in Prism 6 (GraphPad) with 40 segments

520   over the 24 hour period (including the ZT 0 timepoint repeated at ZT 24) for increments of 0.615385

521   hours. For mice, cubic spline interpolation was performed with 36 segments for increments of

522   0.6857143 hours. For analysis, the maximum disc shedding rate during both the morning and

523   evening was determined as the peak of disc shedding. To calculate the digestion rates of

524   phagosomes, the maximum and minimum points of disc shedding for both the morning and

525   evening shedding events was determined. Rates of phagosome digestion were subsequently

526   calculated as the decreasing slope of the number of phagosomes over the period of between 25%

527   and 75% of the total time between maximum and minimum. Phagosome half-life was calculated

20

528   for both morning and evening as the time after the maximum peak until the phagosome number

529   reached half-way between the maximum and minimum points.

530

531   **Immunogold labeling**

532   For immunogold analysis, 7dpf transgenic larvae were collected at 1.5 hours after light onset or

533   14dpf wild-type larvae were collected at both 1.5 hours after light onset and 1.5 hours after dark

534   onset. Larvae were fixed overnight in 0.1% glutaraldehyde and 2% paraformaldehyde in 0.1M

535   phosphate buffer (pH 7.4). Larvae were washed in phosphate buffer, dehydrated with two 30

536   minute washes of 70% ethanol, and incubated with a 2:1 mixture of LR white:70% ethanol for 1

537   hour. Larvae were then incubated overnight in LR white at room temperature. In the morning,

538   following two 30 minute changes of LR white, larvae were embedded and polymerized at 55°C for

539   48 hours. Ultra-thin sections were mounted on 200 mesh formvar/carbon coated copper grids.

540   Grids were incubated on drops of 0.15 mM glycine for 10 minutes, then on 5% BSA in 0.1M

541   phosphate buffer for 15 minutes. For labeling, grids were incubated on drops of antibody for 90

542   minutes. Grids were washed in 5% BSA in 0.1M phosphate buffer and incubated with colloidal gold

543   secondary (Electron Microscopy Sciences) for 1 hour. Grids were washed in double-distilled H_2O

544   and stained with 1% aqueous uranyl acetate for 2 minutes. For each analysis, a total of five larvae

545   were analyzed for each condition. For analysis, the number of both gold-labeled and unlabeled

546   phagosomes was counted and divided by the total length of RPE measured.

547

548   **qPCR analysis**

549   For mouse circadian *Kif17* expression analysis, adult C57BL/6 mouse retinas were collected every

550   four hours beginning at light onset over a 24 hour period and placed RNAlater (Ambion) overnight

551   at 4°C. For zebrafish circadian *kif17* expression analysis, 14dpf ZDR zebrafish eyes were collected

552   at nine discrete timepoints following light onset: 0 (light onset), 1.5 hours, 3.5 hours, 7.5 hours,

553   10.5 hours, 14 hours (dark), 15.5 hours, 17.5 hours, 20.5 hours. For each biological replicate, three

21

554   zebrafish eyes were pooled. For zebrafish opsin expression analysis, five whole 7dpf zebrafish

555   larvae were pooled. Following sample collection, RNA was extracted, cDNA synthesized, and

556   qPCR run as previously described [14]. For each data-point, three biological replicates were run

557   in triplicate for both mouse and zebrafish samples. For mouse, published *Kif17* primers were used

558   [46] and published RNA polymerase II primers were used as a reference gene [47]. For zebrafish,

559   published ef1α primers were used as a reference gene [14], published opsin primers were used

560   [14], and *kif17* primers are depicted below.

Primer	Sequence	Efficiency
kif17 (F)	GGATGAAGAGGGAGGAAC	98.5%
kif17 (R)	CAATGACACCAGAAGGAG	

561

562   All expression values were standardized to 1 for the light onset timepoint (ZT 0).

563

564   **Imaging**

565   Immunofluorescent images were acquired with a 100x, 1.30 NA oil-immersion lens (Nikon) on

566   either an Eclipse TE300 (Nikon) microscope operating NIS-Elements (Nikon) and a Zyla sCMOS

567   camera (Andor) or a C1 Plus-EX3 AOM Confocal System (Nikon) operating EZ-C1 (Nikon). TEM

568   imaging was performed on a Hitachi H-600 with an ORCA-100 digital camera (Hamamatsu).

569   Blinded image analysis was performed on de-identified, randomized images with ImageJ.

570

571   **Statistical analysis**

572   For ciliary and nuclear localization of KIF17 in mammalian cell culture experiments, a one-way

573   ANOVA was performed. Following significance, a Bonferroni multiple-comparisons post-hoc test

574   was performed to determine significance between groups. For OS localization frequency and

575   nuclear localization in zebrafish photoreceptors, a one-way ANOVA was performed. For line

576   intensity analysis, a two-way ANOVA was performed. For single-timepoint disc shedding analysis

577   in transgenic or injected larvae, a one-way ANOVA was performed. For immunogold phagosomes

578   analysis in either transgenic or wild-type larvae, a two-way ANOVA was performed. For circadian

579   disc shedding analysis in either zebrafish or mice, a two-way ANOVA was performed. For circadian

580   *Kif17* mRNA expression in either mouse or zebrafish retinas, a one-way ANOVA was performed.

581   For qPCR analysis of opsin expression, a one-way ANOVA was performed for each opsin gene.

582   For all experiments, following significance with either one-way or two-way ANOVA, a Bonferroni

583   multiple-comparisons post-hoc test was performed to determine significance between groups. For

584   all experiments, values are expressed as mean ± SEM and significance is labeled as * : $p \leq .05$,

585   **: $p \leq .01$, ***: $p \leq .001$, ****: $p \leq .0001$. Non-significant values are unlabeled.

586

587   **Abbreviations**

588   RPE = retinal pigment epithelium
589   NLS = nuclear localization signal
590   CLS = ciliary localization signal
591   OS = outer segment
592   PS = phosphatidylserine
593   ZT = Zeitgeber Time
594

595   **Declarations**

596   **Ethics approval and consent to participate**

597   All experiments were approved and conducted in accordance with the Institutional Animal Care

598   and Use Committee of the Medical College of Wisconsin.

599

600   **Consent for publication**

601   Not applicable

602

603   **Availability of data and materials**

604   All data generated or analysed during this study are included in this published article and its

605   supplkementary information files.

606

Competing interests

608   The authors declare that they have no competing interests.

609

Funding

615

Authors' contributions

617   TRL, CI, and JCB designed experiments. TRL, CI, and SRK, performed experiments. TRL, BAL,

618   and JCB analyzed data. TRL and JCB wrote the initial manuscript. All authors read and approved

619   the final manuscript.

620

Acknowledgements

622   Not applicable

623

References

625   1.   Satir P, Christensen ST. Overview of structure and function of mammalian cilia. Annual
626   review   of   physiology.   2007;69:377-400.   Epub   2006/10/03.   doi:
627   10.1146/annurev.physiol.69.040705.141236. PubMed PMID: 17009929.

628   2.   Waters AM, Beales PL. Ciliopathies: an expanding disease spectrum. Pediatric nephrology
629   (Berlin, Germany). 2011;26(7):1039-56. Epub 2011/01/07. doi: 10.1007/s00467-010-1731-7.
630   PubMed PMID: 21210154; PubMed Central PMCID: PMCPMC3098370.

631   3.   Szymanska K, Johnson CA. The transition zone: an essential functional compartment of
632   cilia. Cilia. 2012;1(1):10. Epub 2013/01/29. doi: 10.1186/2046-2530-1-10. PubMed PMID:
633   23352055; PubMed Central PMCID: PMCPMC3555838.

634   4.   Breslow DK, Koslover EF, Seydel F, Spakowitz AJ, Nachury MV. An in vitro assay for entry
635   into cilia reveals unique properties of the soluble diffusion barrier. The Journal of cell biology.
636   2013;203(1):129-47. Epub 2013/10/09. doi: 10.1083/jcb.201212024. PubMed PMID: 24100294;
637   PubMed Central PMCID: PMCPMC3798247.

638   5.   Kee HL, Dishinger JF, Blasius TL, Liu CJ, Margolis B, Verhey KJ. A size-exclusion
639   permeability barrier and nucleoporins characterize a ciliary pore complex that regulates transport
640   into cilia. Nature cell biology. 2012;14(4):431-7. Epub 2012/03/06. doi: 10.1038/ncb2450. PubMed
641   PMID: 22388888; PubMed Central PMCID: PMCPMC3319646.

642   6.   Dishinger JF, Kee HL, Jenkins PM, Fan S, Hurd TW, Hammond JW, et al. Ciliary entry of
643   the kinesin-2 motor KIF17 is regulated by importin-beta2 and RanGTP. Nature cell biology.
644   2010;12(7):703-10. Epub 2010/06/08. doi: 10.1038/ncb2073. PubMed PMID: 20526328; PubMed
645   Central PMCID: PMCPMC2896429.

646   7.   Funabashi T, Katoh Y, Michisaka S, Terada M, Sugawa M, Nakayama K. Ciliary entry of
647   KIF17 is dependent on its binding to the IFT-B complex via IFT46-IFT56 as well as on its nuclear
648   localization signal. Molecular biology of the cell. 2017;28(5):624-33. Epub 2017/01/13. doi:
649   10.1091/mbc.E16-09-0648. PubMed PMID: 28077622; PubMed Central PMCID:
650   PMCPMC5328621.

651   8.   Wong-Riley MT, Besharse JC. The kinesin superfamily protein KIF17: one protein with
652   many functions. Biomolecular concepts. 2012;3(3):267-82. Epub 2013/06/14. doi: 10.1515/bmc-
653   2011-0064. PubMed PMID: 23762210; PubMed Central PMCID: PMCPMC3677786.

654   9.   Macho B, Brancorsini S, Fimia GM, Setou M, Hirokawa N, Sassone-Corsi P. CREM-
655   dependent transcription in male germ cells controlled by a kinesin. Science (New York, NY).
656   2002;298(5602):2388-90. Epub 2002/12/21. doi: 10.1126/science.1077265. PubMed PMID:
657   12493914.

658   10.   Seneviratne A, Turan Z, Hermant A, Lecine P, Smith WO, Borg JP, et al. Modulation of
659   estrogen related receptor alpha activity by the kinesin KIF17. Oncotarget. 2017. Epub 2017/06/10.
660   doi: 10.18632/oncotarget.18104. PubMed PMID: 28596477.

661   11.   Guillaud L, Wong R, Hirokawa N. Disruption of KIF17-Mint1 interaction by CaMKII-
662   dependent phosphorylation: a molecular model of kinesin-cargo release. Nature cell biology.
663   2008;10(1):19-29. Epub 2007/12/11. doi: 10.1038/ncb1665. PubMed PMID: 18066053.

664   12.   Insinna C, Pathak N, Perkins B, Drummond I, Besharse JC. The homodimeric kinesin,
665   Kif17, is essential for vertebrate photoreceptor sensory outer segment development.
666   Developmental biology. 2008;316(1):160-70. Epub 2008/02/29. doi: 10.1016/j.ydbio.2008.01.025.
667   PubMed PMID: 18304522; PubMed Central PMCID: PMCPMC2362383.

668   13.   Rohlich P. The sensory cilium of retinal rods is analogous to the transitional zone of motile
669   cilia. Cell and tissue research. 1975;161(3):421-30. Epub 1975/08/25. PubMed PMID: 1175211.

670   14.   Lewis TR, Kundinger SR, Pavlovich AL, Bostrom JR, Link BA, Besharse JC. Cos2/Kif7 and
671   Osm-3/Kif17 regulate onset of outer segment development in zebrafish photoreceptors through
672   distinct mechanisms. Developmental biology. 2017;425(2):176-90. Epub 2017/03/28. doi:
673   10.1016/j.ydbio.2017.03.019. PubMed PMID: 28341548.

674   15.   Jiang L, Tam BM, Ying G, Wu S, Hauswirth WW, Frederick JM, et al. Kinesin family 17
675   (osmotic avoidance abnormal-3) is dispensable for photoreceptor morphology and function.
676   FASEB journal : official publication of the Federation of American Societies for Experimental
677   Biology. 2015;29(12):4866-80. Epub 2015/08/01. doi: 10.1096/fj.15-275677. PubMed PMID:
678   26229057; PubMed Central PMCID: PMCPMC4653055.

679   16.   Bader JR, Kusik BW, Besharse JC. Analysis of KIF17 distal tip trafficking in zebrafish cone
680   photoreceptors. Vision research. 2012;75:37-43. Epub 2012/10/27. doi:
681   10.1016/j.visres.2012.10.009. PubMed PMID: 23099049; PubMed Central PMCID:
682   PMCPMC3556995.

683   17.   Williams CL, McIntyre JC, Norris SR, Jenkins PM, Zhang L, Pei Q, et al. Direct evidence
684   for BBSome-associated intraflagellar transport reveals distinct properties of native mammalian
685   cilia. Nature communications. 2014;5:5813. Epub 2014/12/17. doi: 10.1038/ncomms6813.
686   PubMed PMID: 25504142; PubMed Central PMCID: PMCPMC4284812.

687   18.   Young RW, Bok D. Participation of the retinal pigment epithelium in the rod outer segment
688   renewal process. The Journal of cell biology. 1969;42(2):392-403. Epub 1969/08/01. PubMed
689   PMID: 5792328; PubMed Central PMCID: PMCPMC2107669.

690   19.   Ruggiero L, Connor MP, Chen J, Langen R, Finnemann SC. Diurnal, localized exposure of
691   phosphatidylserine by rod outer segment tips in wild-type but not Itgb5-/- or Mfge8-/- mouse retina.
692   Proceedings of the National Academy of Sciences of the United States of America.
693   2012;109(21):8145-8. Epub 2012/05/09. doi: 10.1073/pnas.1121101109. PubMed PMID:
694   22566632; PubMed Central PMCID: PMCPMC3361434.

695   20.   Adamus G, Arendt A, Hargrave PA. Genetic control of antibody response to bovine
696   rhodopsin in mice: epitope mapping of rhodopsin structure. Journal of neuroimmunology.
697   1991;34(2-3):89-97. Epub 1991/11/01. PubMed PMID: 1717506.

698   21.   LaVail MM. Rod outer segment disk shedding in rat retina: relationship to cyclic lighting.
699   Science (New York, NY). 1976;194(4269):1071-4. Epub 1976/12/03. PubMed PMID: 982063.

700   22.   O'Day WT, Young RW. Rhythmic daily shedding of outer-segment membranes by visual
701   cells in the goldfish. The Journal of cell biology. 1978;76(3):593-604. Epub 1978/03/01. PubMed
702   PMID: 632320; PubMed Central PMCID: PMCPMC2110002.

703   23.   Ko GY, Ko ML, Dryer SE. Circadian regulation of cGMP-gated cationic channels of chick
704   retinal cones. Erk MAP Kinase and Ca2+/calmodulin-dependent protein kinase II. Neuron.
705   2001;29(1):255-66. Epub 2001/02/22. PubMed PMID: 11182096.

706   24.   Hayashi Y, Shi SH, Esteban JA, Piccini A, Poncer JC, Malinow R. Driving AMPA receptors
707   into synapses by LTP and CaMKII: requirement for GluR1 and PDZ domain interaction. Science
708   (New York, NY). 2000;287(5461):2262-7. Epub 2000/03/24. PubMed PMID: 10731148.

709   25.   Honnappa S, Gouveia SM, Weisbrich A, Damberger FF, Bhavesh NS, Jawhari H, et al. An
710   EB1-binding motif acts as a microtubule tip localization signal. Cell. 2009;138(2):366-76. Epub
711   2009/07/28. doi: 10.1016/j.cell.2009.04.065. PubMed PMID: 19632184.

712   26.   Jaulin F, Kreitzer G. KIF17 stabilizes microtubules and contributes to epithelial
713   morphogenesis by acting at MT plus ends with EB1 and APC. The Journal of cell biology.
714   2010;190(3):443-60. Epub 2010/08/11. doi: 10.1083/jcb.201006044. PubMed PMID: 20696710;
715   PubMed Central PMCID: PMCPMC2922650.

716   27.   Schroder JM, Schneider L, Christensen ST, Pedersen LB. EB1 is required for primary cilia
717   assembly in fibroblasts. Current biology : CB. 2007;17(13):1134-9. Epub 2007/06/30. doi:
718   10.1016/j.cub.2007.05.055. PubMed PMID: 17600711.

719   28.   Zhao C, Omori Y, Brodowska K, Kovach P, Malicki J. Kinesin-2 family in vertebrate
720   ciliogenesis. Proceedings of the National Academy of Sciences of the United States of America.
721   2012;109(7):2388-93. Epub 2012/02/07. doi: 10.1073/pnas.1116035109. PubMed PMID:
722   22308397; PubMed Central PMCID: PMCPMC3289367.

723   29.   Pooranachandran N, Malicki JJ. Unexpected Roles for Ciliary Kinesins and Intraflagellar
724   Transport   Proteins.   Genetics.   2016;203(2):771-85.   Epub   2016/04/03.   doi:
725   10.1534/genetics.115.180943.   PubMed   PMID: 27038111;   PubMed   Central   PMCID:
726   PMCPMC4896193.

727   30.   Finnemann SC, Bonilha VL, Marmorstein AD, Rodriguez-Boulan E. Phagocytosis of rod
728   outer segments by retinal pigment epithelial cells requires alpha(v)beta5 integrin for binding but
729   not for internalization. Proceedings of the National Academy of Sciences of the United States of
730   America. 1997;94(24):12932-7. Epub 1997/11/25. PubMed PMID: 9371778; PubMed Central
731   PMCID: PMCPMC24241.

732   31.   Feng W, Yasumura D, Matthes MT, LaVail MM, Vollrath D. Mertk triggers uptake of
733   photoreceptor outer segments during phagocytosis by cultured retinal pigment epithelial cells. The
734   Journal of biological chemistry. 2002;277(19):17016-22. Epub 2002/02/28. doi:
735   10.1074/jbc.M107876200. PubMed PMID: 11861639.

736   32.   Bulloj A, Duan W, Finnemann SC. PI 3-kinase independent role for AKT in F-actin
737   regulation during outer segment phagocytosis by RPE cells. Experimental eye research.
738   2013;113:9-18. Epub 2013/05/15. doi: 10.1016/j.exer.2013.05.002. PubMed PMID: 23669303;
739   PubMed Central PMCID: PMCPMC3737417.

740   33.   LaVail MM. Kinetics of rod outer segment renewal in the developing mouse retina. The
741   Journal of cell biology. 1973;58(3):650-61. Epub 1973/09/01. PubMed PMID: 4747920; PubMed
742   Central PMCID: PMCPMC2109077.

743   34.   Young RW. The renewal of photoreceptor cell outer segments. The Journal of cell biology.
744   1967;33(1):61-72. Epub 1967/04/01. PubMed PMID: 6033942; PubMed Central PMCID:
745   PMCPMC2107286.

746   35.   Willoughby JJ, Jensen AM. Generation of a genetically encoded marker of rod
747   photoreceptor outer segment growth and renewal. Biology open. 2012;1(1):30-6. Epub
748   2012/12/06. doi: 10.1242/bio.2011016. PubMed PMID: 23213365; PubMed Central PMCID:
749   PMCPMC3507166.

750   36.   Frasch SC, Henson PM, Kailey JM, Richter DA, Janes MS, Fadok VA, et al. Regulation of
751   phospholipid scramblase activity during apoptosis and cell activation by protein kinase Cdelta. The
752   Journal of biological chemistry. 2000;275(30):23065-73. Epub 2000/04/20. doi:
753   10.1074/jbc.M003116200. PubMed PMID: 10770950.

754   37.   Hankins HM, Baldridge RD, Xu P, Graham TR. Role of flippases, scramblases and transfer
755   proteins in phosphatidylserine subcellular distribution. Traffic (Copenhagen, Denmark).
756   2015;16(1):35-47. Epub 2014/10/07. doi: 10.1111/tra.12233. PubMed PMID: 25284293; PubMed
757   Central PMCID: PMCPMC4275391.

758   38.   Bulloj A, Maminishkis A, Mizui M, Finnemann SC. Semaphorin4D-PlexinB1 Signaling
759   Attenuates Photoreceptor Outer Segment Phagocytosis by Reducing Rac1 Activity of RPE Cells.
760   Molecular neurobiology. 2017. Epub 2017/06/19. doi: 10.1007/s12035-017-0649-5. PubMed
761   PMID: 28624895.

762   39.   Besharse JC, Hollyfield JG, Rayborn ME. Photoreceptor outer segments: accelerated
763   membrane renewal in rods after exposure to light. Science (New York, NY). 1977;196(4289):536-
764   8. Epub 1977/04/29. PubMed PMID: 300504.

765 40. Young RW. The daily rhythm of shedding and degradation of rod and cone outer segment
766 membranes in the chick retina. Investigative ophthalmology & visual science. 1978;17(2):105-16.
767 Epub 1978/02/01. PubMed PMID: 624604.

768 41. Long KO, Fisher SK, Fariss RN, Anderson DH. Disc shedding and autophagy in the cone-
769 dominant ground squirrel retina. Experimental eye research. 1986;43(2):193-205. Epub
770 1986/08/01. PubMed PMID: 3758219.

771 42. Carter-Dawson LD, LaVail MM. Rods and cones in the mouse retina. I. Structural analysis
772 using light and electron microscopy. The Journal of comparative neurology. 1979;188(2):245-62.
773 Epub 1979/11/15. doi: 10.1002/cne.901880204. PubMed PMID: 500858.

774 43. Kennedy BN, Alvarez Y, Brockerhoff SE, Stearns GW, Sapetto-Rebow B, Taylor MR, et al.
775 Identification of a zebrafish cone photoreceptor-specific promoter and genetic rescue of
776 achromatopsia in the nof mutant. Investigative ophthalmology & visual science. 2007;48(2):522-9.
777 Epub 2007/01/26. doi: 10.1167/iovs.06-0975. PubMed PMID: 17251445.

778 44. Kawakami K. Tol2: a versatile gene transfer vector in vertebrates. Genome biology. 2007;8
779 Suppl 1:S7. Epub 2007/12/06. doi: 10.1186/gb-2007-8-s1-s7. PubMed PMID: 18047699; PubMed
780 Central PMCID: PMCPMC2106836.

781 45. Vihtelic TS, Doro CJ, Hyde DR. Cloning and characterization of six zebrafish photoreceptor
782 opsin cDNAs and immunolocalization of their corresponding proteins. Visual neuroscience.
783 1999;16(3):571-85. Epub 1999/06/01. PubMed PMID: 10349976.

784 46. Wong RW, Setou M, Teng J, Takei Y, Hirokawa N. Overexpression of motor protein KIF17
785 enhances spatial and working memory in transgenic mice. Proceedings of the National Academy
786 of Sciences of the United States of America. 2002;99(22):14500-5. Epub 2002/10/23. doi:
787 10.1073/pnas.222371099. PubMed PMID: 12391294; PubMed Central PMCID: PMCPMC137912.

788 47. Sodhi CP, Li J, Duncan SA. Generation of mice harbouring a conditional loss-of-function
789 allele of Gata6. BMC developmental biology. 2006;6:19. Epub 2006/04/14. doi: 10.1186/1471-
790 213x-6-19. PubMed PMID: 16611361; PubMed Central PMCID: PMCPMC1481595.
791

792

793

794
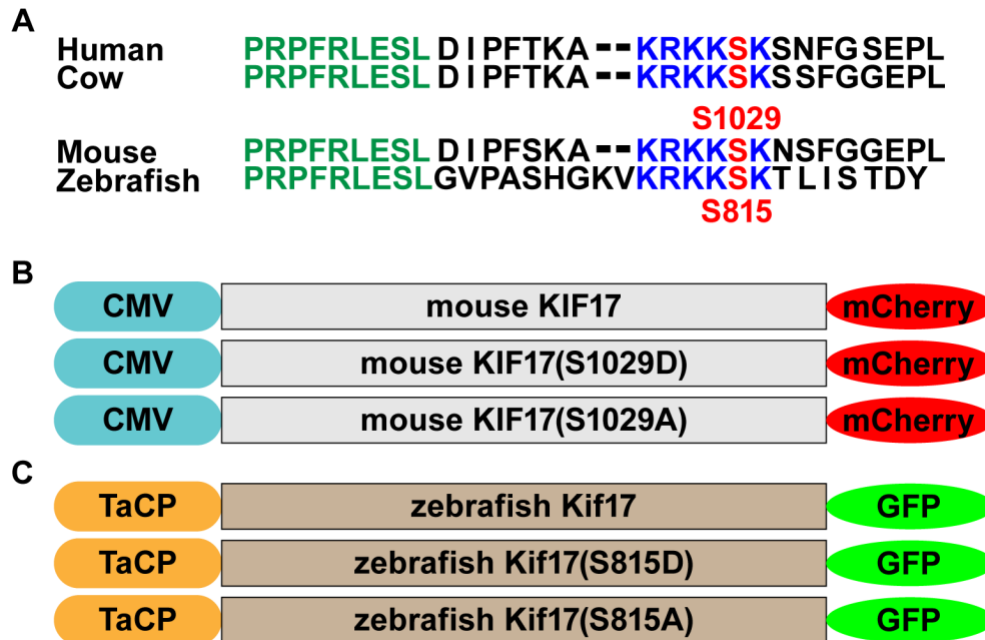
Figure 1. Schematic of transgenic phospho-mutant KIF17 constructs

(A) The amino acid sequence of the C-terminus of KIF17 in various species is depicted. Homologous sequences are shown in color (green, blue, and red). The green conserved sequence has been shown to interact with the IFT-B complex [7], while the blue conserved sequence functions as a NLS or CLS [6]. The conserved serine (red), mouse S1029/zebrafish S815, has been shown to be phosphorylated by CaMKII [11]. **(B)** For mammalian cell culture experiments, three different mCherry-tagged constructs of mouse KIF17 under control of the ubiquitous CMV promoter were generated: wild-type KIF17, phospho-mimetic KIF17(S1029D), and phospho-deficient KIF17(S1029A). (**C**) For zebrafish cone photoreceptor experiments, three different GFP-tagged constructs of zebrafish under control of the cone-specific transducin-α promoter (TaCP) were generated: wild-type Kif17, phospho-mimetic Kif17(S815D), and phospho-deficient Kif17(S815A).
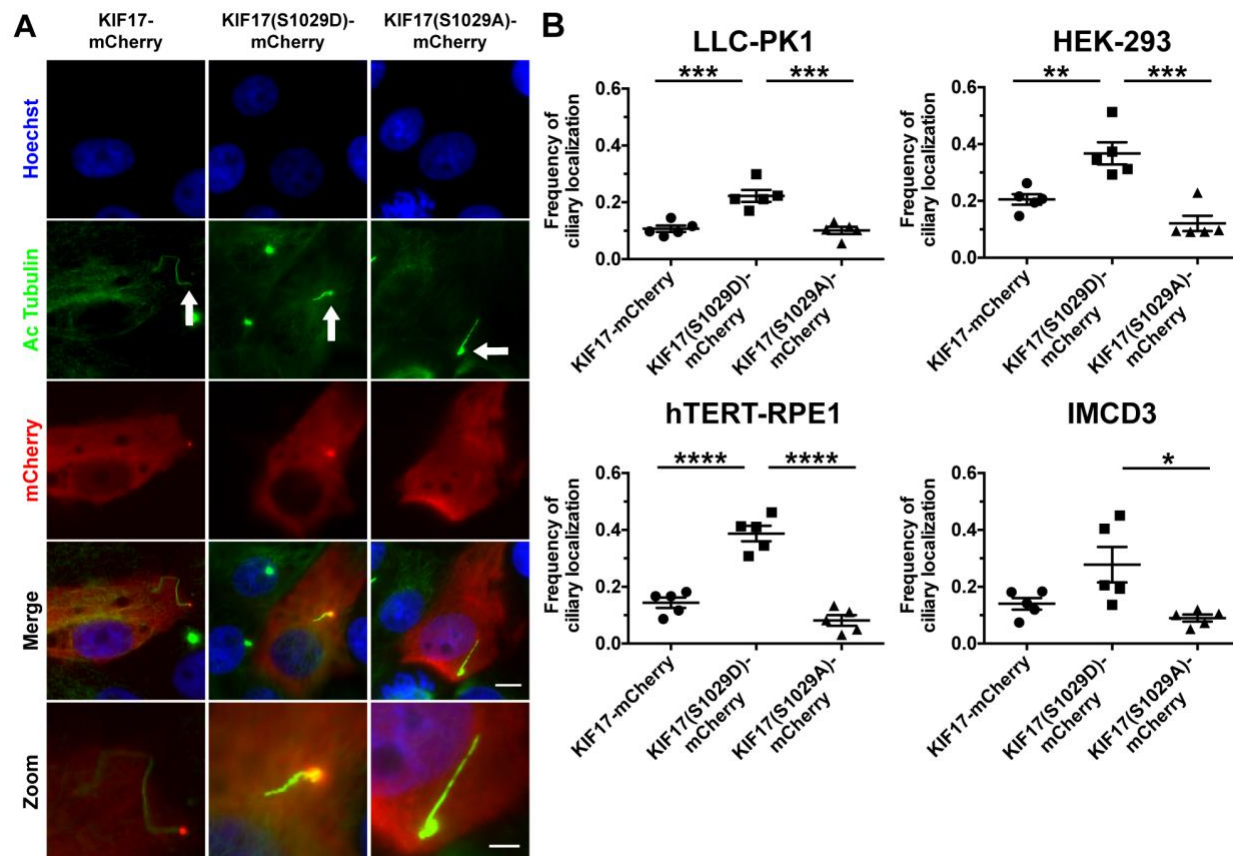
Figure 2. Phospho-mutations of S1029 regulate ciliary localization of KIF17

(A) LLC-PK1 cells were serum-starved to induce ciliogenesis and transfected with either KIF17-mCherry (top), KIF17(S1029D)-mCherry (middle), or KIF17(S1029A)-mCherry (bottom). 24 hours following transfection, cells were stained with Hoechst (blue) to label nuclei and acetylated α-tubulin (green) to label axonemes. The arrows mark the cilia. The zoom panel depicts a high-magnification of the cilium. Of note, transgenic KIF17 accumulates within the cilia (arrows), presumably at the ciliary tip as observed previously [6] [7] [15]. Cilia are often twisted and non-linear. Additionally, there is generally significantly less nuclear than cytoplasmic localization of each KIF17 transgene. Scale bar is 10 μm for normal magnification images. Scale bar is 4 μm for zoom panel. **(B)** Quantification of frequency of ciliary localization of each transgene 24 hours post-transfection in various mammalian ciliated cell lines. In LLC-PK1 cells, ciliary localization of KIF17-mCherry (n=5 transfections, 710 cells), KIF17(S1029D)-mCherry (n=5, 859 cells), and

31

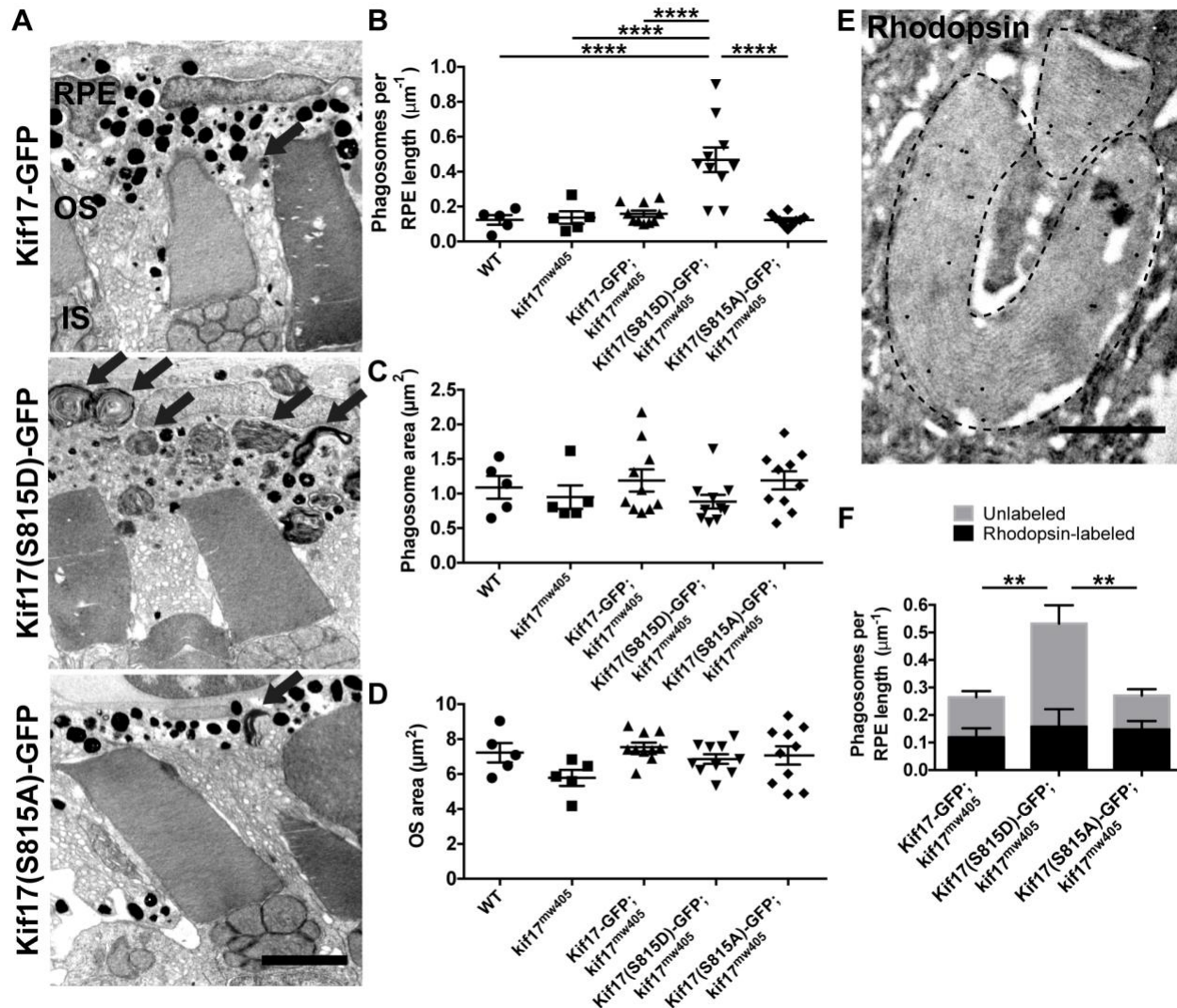824   KIF17(S1029A)-mCherry (n=5, 664 cells) is shown. In HEK-293 cells, ciliary localization of KIF17-

825   mCherry (n=5 transfections, 690 cells), KIF17(S1029D)-mCherry (n=5, 1149 cells), and

826   KIF17(S1029A)-mCherry (n=5, 886 cells) is shown. In hTERT-RPE1 cells, ciliary localization of

827   KIF17-mCherry (n=5 transfections, 280 cells), KIF17(S1029D)-mCherry (n=5, 307 cells), and

828   KIF17(S1029A)-mCherry (n=5, 279 cells) is shown. In IMCD3 cells, ciliary localization of KIF17-

829   mCherry (n=5 transfections, 665 cells), KIF17(S1029D)-mCherry (n=5, 815 cells), and

830   KIF17(S1029A)-mCherry (n=5, 845 cells) is shown.

831

832

833

834

835

836

837

838

839

840

841

842

843

844

845

846

847

848

849
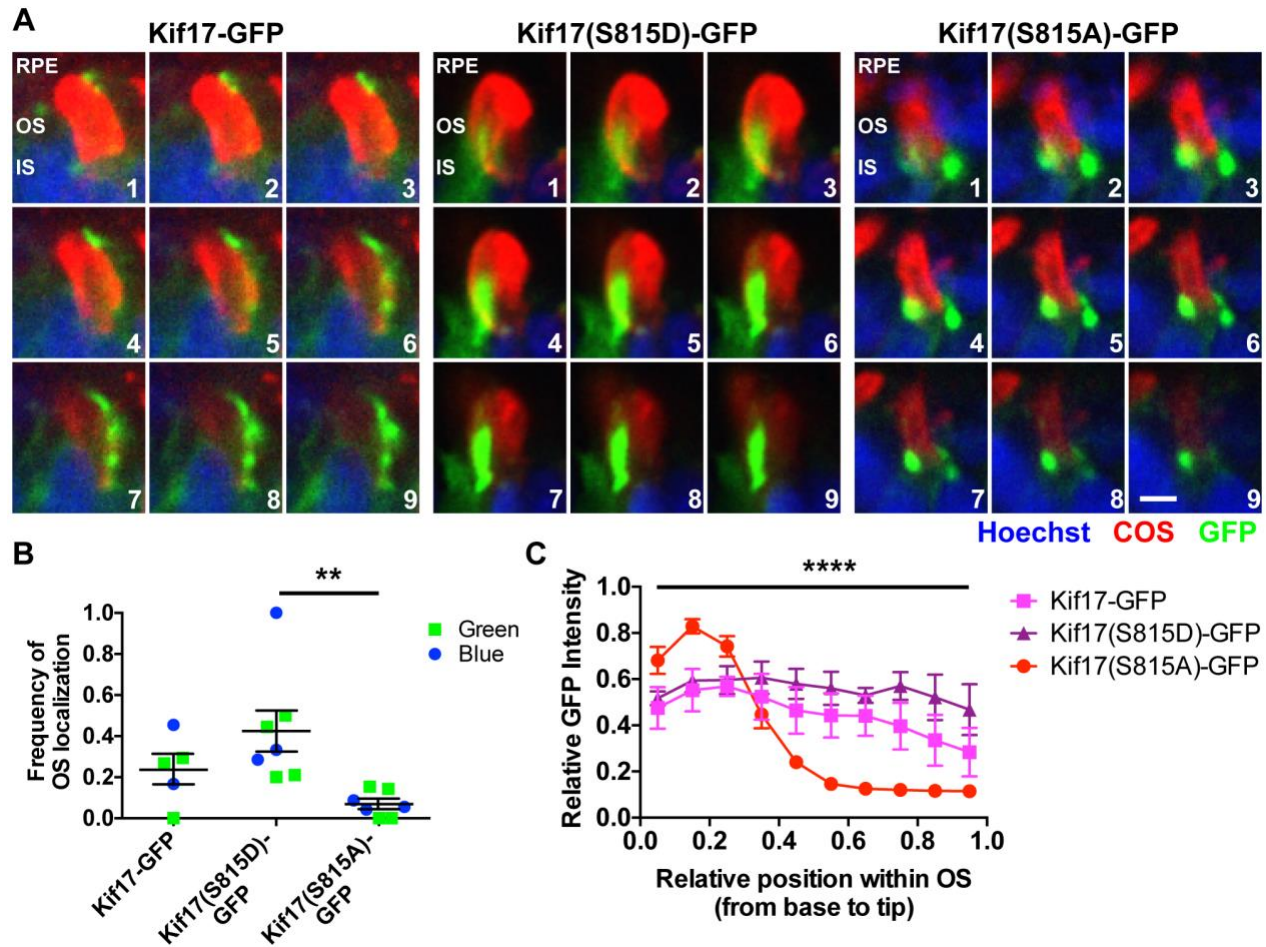
Figure 3. Phospho-mutations of S815 regulate photoreceptor OS localization of Kif17

(A) 5 dpf larvae previously injected at the one cell stage with one of three different transgenic constructs under control of the TaCP promoter for expression in cone photoreceptors: Kif17-GFP (left), phospho-mimetic Kif17(S815D)-GFP (middle), and phospho-deficient Kif17(S815A)-GFP (right) were stained with Hoechst (blue) to label nuclei and blue cone opsin (red) to label cone OS. A z-series of confocal images was taken with 0.2 μm steps through the depth of the photoreceptor OS. Shown are montages of sequential images in the z-series revealing that Kif17(S815D)-GFP exhibits significant accumulation in the OS while Kif17(S815A)-GFP accumulates at the base of the OS. Note that in cone photoreceptors, the ciliary axoneme extends along the side of the opsin-containing discs. Scale bar is 1 μm. **(B)** Quantification of the frequency of OS accumulation of Kif17-GFP (n=5 total injected larvae: 3 stained for green opsin, 2 stained for blue opsin; 60 cells),

862   Kif17(S815D)-GFP (n=7: 4 green, 3 blue; 62 cells), and Kif17(S815A)-GFP (n=7: 4 green, 3 blue;

863   126 cells) when co-labeled with either green opsin (square) or blue opsin (circle). **(C)** Line intensity

864   analysis of the GFP signal for Kif17-GFP (pink line, n=5 total injected larvae: 3 stained for green

865   opsin, 2 stained for blue opsin; 17 cells), Kif17(S815D)-GFP (purple line, n=5: 3 green, 2 blue; 17

866   cells), and Kif17(S815A)-GFP (red line, n=5: 3 green, 2 blue; 25 cells). Two-way ANOVA was

867   performed to determine significance in the different interaction between GFP signal intensity

868   pattern and transgene (p<0.0001, ****).

869

870

871

872

873

874

875

876

877

878

879

880

881

882

883

884

885

886

887

888

Figure 4. Phospho-mimetic Kif17(S815D) increases disc shedding

890 **(A)** TEM images of 7dpf $kif17^{mw405}$ larvae that are stably expressing either Kif17-GFP (left),

891 phospho-mimetic Kif17(S815D)-GFP (middle), or phospho-deficient Kif17(S815A)-GFP (right) in

892 cones collected at ZT 1.5. Black arrows indicate phagosomes. Scale bar is 2 μm. IS is inner

893 segment. **(B)** Quantification of the number of phagosomes for wild-type (n=5 larvae, 1273 μm of

894 RPE); $kif17^{mw405}$ (n=5, 1170 μm of RPE); Kif17-GFP, $kif17^{mw405}$ (n=10, 2677 μm of RPE);

895 Kif17(S815D)-GFP, $kif17^{mw405}$ (n=10, 2938 μm of RPE); and Kif17(S815A)-GFP, $kif17^{mw405}$ (n=10,

896 2875 μm of RPE) larvae. **(C)** Quantification of the area of phagosomes for wild-type (n=5 larvae,

897 403 phagosomes); $kif17^{mw405}$ (n=5, 392 phagosomes); Kif17-GFP, $kif17^{mw405}$ (n=10, 530

35

898   phagosomes); Kif17(S815D)-GFP, *kif17^{mw405}* (n=10, 1601 phagosomes); and Kif17(S815A)-GFP,

899   *kif17^{mw405}* (n=10, 547 phagosomes) larvae. **(D)** Quantification of OS size for wild-type (n=5 larvae,

900   268 OS); *kif17^{mw405}* (n=5, 255 OS); Kif17-GFP, *kif17^{mw405}* (n=10, 615 OS); Kif17(S815D)-GFP,

901   *kif17^{mw405}* (n=10, 566 OS); and Kif17(S815A)-GFP, *kif17^{mw405}* (n=10, 605 OS) larvae. **(E)**

902   Immunogold labeling of a 7 dpf TaCP:Kif17-GFP zebrafish retina with K62-171c, an antibody

903   against bovine rhodopsin showing a positive labeling of a phagosome, as also depicted in **Figure**

904   **S7**. Scale bar is 0.5 µm. **(F)** Analysis of immunogold labeling of rhodopsin-containing or unlabeled

905   phagosomes in 7 dpf Kif17-GFP, *kif17^{mw405}* (n=5 larvae, 1031 µm of RPE); Kif17(S815D)-GFP,

906   *kif17^{mw405}* (n=5, 1268 µm of RPE); and Kif17(S815A)-GFP, *kif17^{mw405}* (n=5, 889 µm of RPE) larvae.

907   Two-way ANOVA was performed to determine significance in the interaction between the

908   transgene expressed and the concentration of rod or cone phagosomes (p=0.0264, *) as well as

909   significance in the total number of phagosomes between transgenes (p=0.0071, **). Bonferroni's

910   multiple comparisons post-hoc test was performed to determine significance in the differences of

911   unlabeled phagosomes between Kif17-GFP and Kif17(S815D)-GFP (p=0.0033, **) and between

912   Kif17(S815A)-GFP and Kif17(S815D)-GFP (p=0.0013, **). There were no differences in numbers

913   of rhodopsin-labeled phagosomes among the transgenes.

914

915

916

917

918

919

920

921

922

923

924
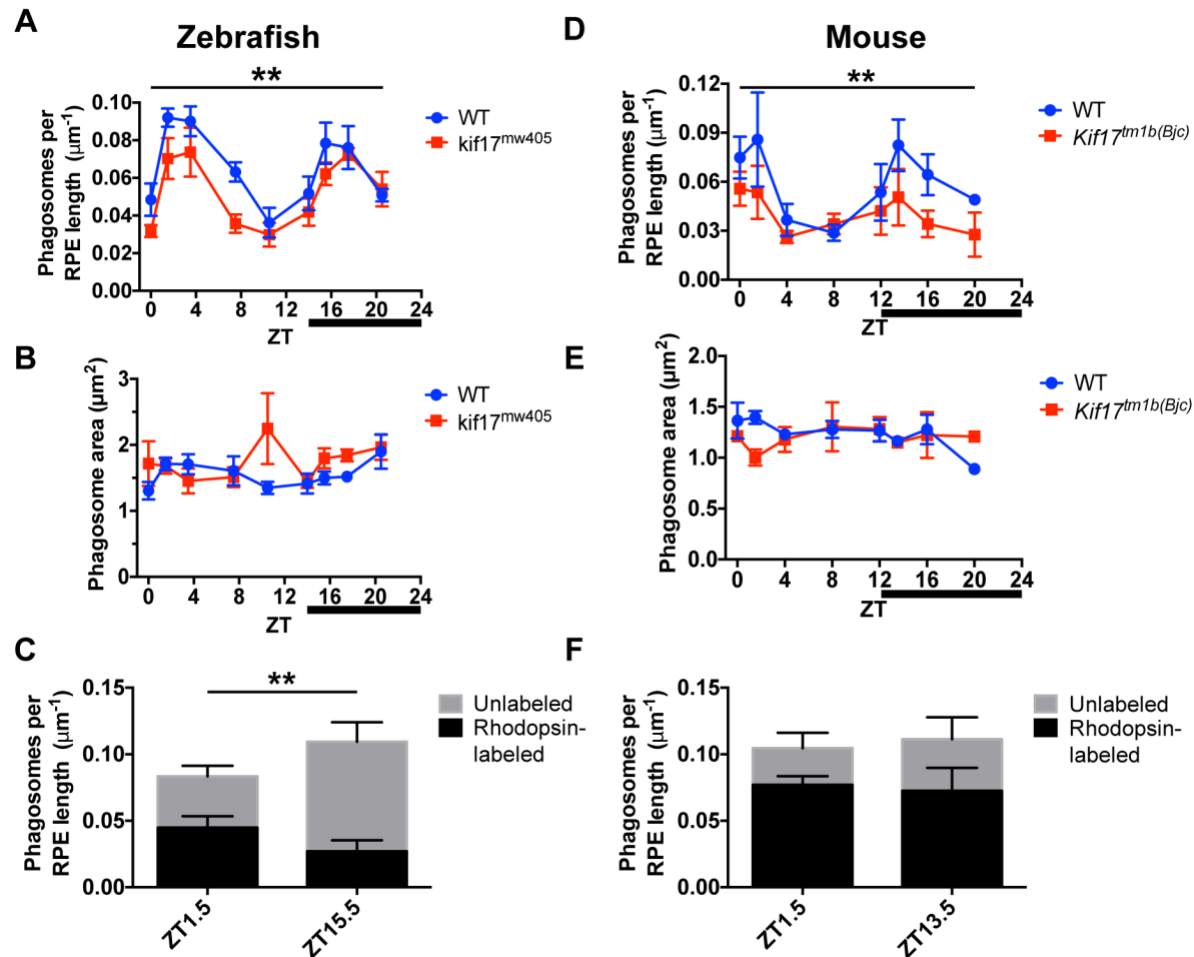
Figure 5. Loss of *kif17* diminishes disc shedding

(A) TEM analysis of phagosome number in 14 dpf wild-type (n=5 larvae at each timepoint, 1400 ± 97 μm of RPE measured at each timepoint) and *kif17^{mw405}* (n=5 larvae at each timepoint, 1469 ± 36 μm of RPE measured at each timepoint) zebrafish collected at nine discrete timepoints following light onset (ZT 0). Dark onset begins at ZT 14 (indicated by dark bar). Two-way ANOVA was performed to determine significance in both phagosome number rhythmicity throughout the timepoints (p<0.0001, ****) as well as between genotypes (p=0.0011, **). **(B)** TEM analysis of phagosome size in 14 dpf wild-type (n=5 larvae at each timepoint, 93 ± 14 phagosomes measured at each timepoint) and *kif17^{mw405}* (n=5 larvae at each timepoint, 79 ± 10 phagosomes measured at each timepoint) zebrafish. **(C)** Immunogold labeling of rhodopsin-containing phagosomes in 14 dpf wild-type retina at either the morning peak of disc shedding, ZT 1.5 (n=5 larvae, 1738 μm of RPE),

37

936   or the evening peak, ZT 15.5 (n=5, 1341 µm of RPE). Two-way ANOVA was performed to

937   determine significance in the interaction between the time of day and the concentration of rod or

938   cone phagosomes (p=0.0082, **). There were no statistical differences in the total number of

939   phagosomes between the morning or night peak. Bonferroni's multiple comparisons post-hoc test

940   was performed to determine significance in the increased of unlabeled phagosomes between

941   morning and night (p=0.0158, *). **(D)** TEM analysis of phagosome number in 2-4 month wild-type

942   (n=3 mice at each timepoint, 979 ± 42 µm of RPE measured at each timepoint) and *Kif17$^{tm1b(Bjc)}$*

943   (n=3 mice at each timepoint, 940 ± 45 µm of RPE measured at each timepoint) mice collected at

944   eight discrete timepoints following light onset (ZT 0). Dark onset begins at ZT 12 (indicated by dark

945   bar). Two-way ANOVA was performed to determine significance in both phagosome number

946   rhythmicity throughout the timepoints (p=0.0300, *) as well as between genotypes (p=0.0096, **).

947   **(E)** TEM analysis of phagosome size in 2-4 month wild-type (n=3 mice at each timepoint, 54 ± 7

948   phagosomes measured at each timepoint) and *Kif17$^{tm1b(Bjc)}$* (n=3 mice at each timepoint, 35 ± 4

949   phagosomes measured at each timepoint) mice. **(F)** Immunogold labeling of rhodopsin-containing

950   phagosomes with B630 rhodopsin antibody in mouse retina at either the morning peak of disc

951   shedding, ZT 1.5 (n=5 mice, 554 µm of RPE), or the evening peak, ZT 13.5 (n=5, 594 µm of RPE).

952   Two-way ANOVA was performed to determine no significance differences in the interaction

953   between the time of day and the concentration of rod or cone phagosomes (p=0.5700) or in the

954   differences in phagosome number between the morning or night peak (p=0.8076), but there was

955   a significant increase in the total number of rod phagosomes compared to cone phagosomes

956   (p=0.0074, **).

957

958

959

960

961
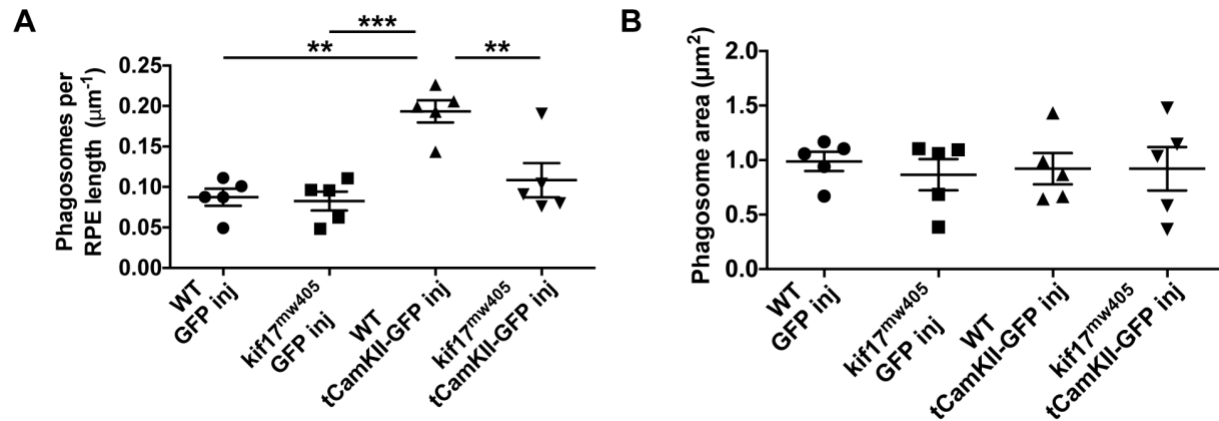
Figure 6. CaMKII promotes *kif17*-dependent disc shedding

(A) TEM phagosome number analysis of 7 dpf GFP-positive wild-type and *kif17^{mw405}* larvae injected with either control TaCP:GFP (n=5 injected larvae, 843 μm of RPE for WT; n=5, 795 μm of RPE for *kif17^{mw405}*) or the constitutively active CaMKII construct TaCP:tCaMKII-GFP (n=5, 1011 μm of RPE for WT; n=5, 1322 μm of RPE for *kif17^{mw405}*). **(B)** Quantification of the size of phagosomes for wild-type and *kif17^{mw405}* larvae injected with either TaCP:GFP (n=5 injected larvae, 74 phagosomes for WT; n=5, 70 phagosomes for *kif17^{mw405}*) or TaCP:tCaMKII-GFP (n=5, 193 phagosomes for WT; n=5, 141 phagosomes for *kif17^{mw405}*).

39

981
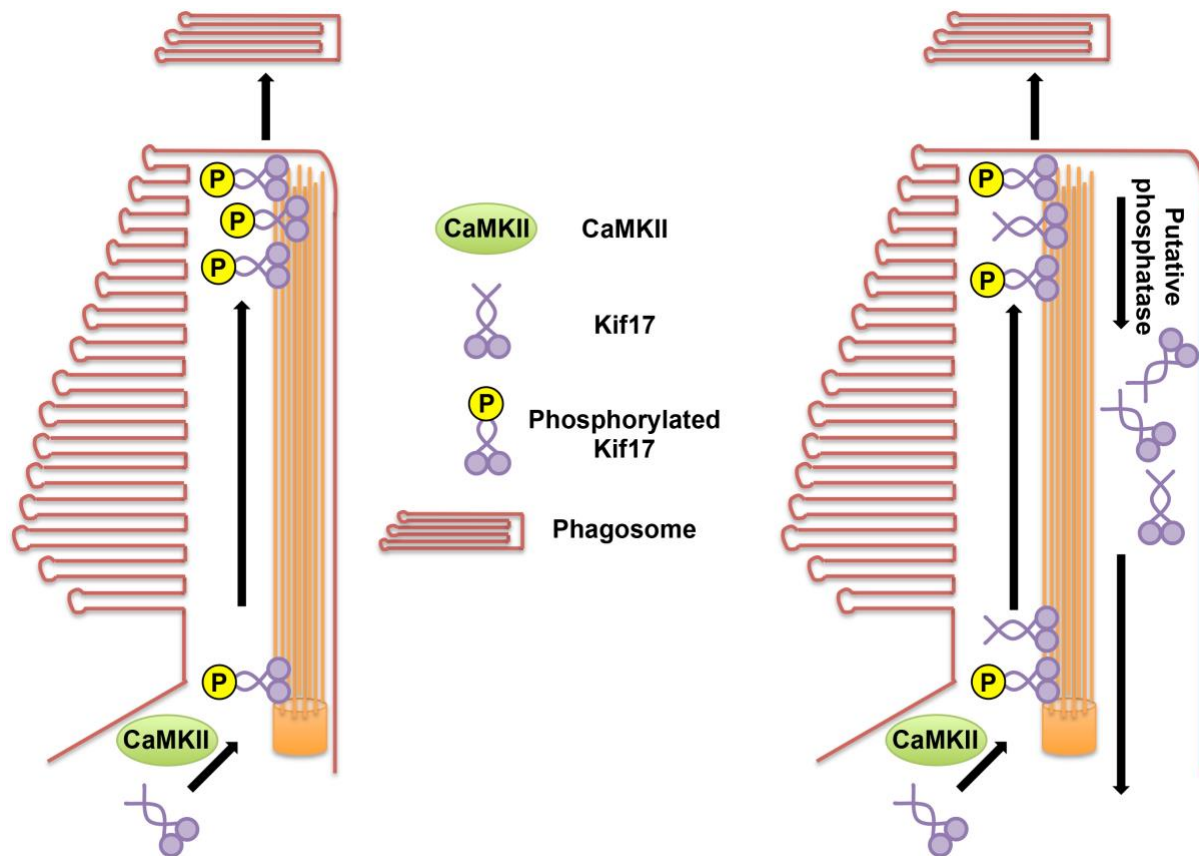
Figure 7. Models of regulation of Kif17 localization through phosphorylation

(Left) In the first model, ciliary localization of Kif17 could be controlled specifically at the transition zone, where only phosphorylated Kif17 (presumably mediated through CaMKII) would enter the cilium. In a photoreceptor, KIF17 in the OS promotes cell-autonomous disc shedding through some putative photoreceptor-centric signaling process. (Right) In a second model, ciliary localization of Kif17 could be controlled not at the transition zone, but rather specifically at the ciliary tip. Both phosphorylated and non-phosphorylated Kif17 could enter the cilium, but non-phosphorylated Kif17 only transiently associates with the axonemal tip. Phosphorylated Kif17 has an enhanced interaction with some putative microtubule associated protein at the axonemal tip, leading to an enhanced ciliary accumulation. A putative phosphatase could regulate Kif17 localization at the ciliary tip, and non-phosphorylated Kif17 could subsequently exit the cilium through either active or passive transport. Similar to the other model, accumulation of Kif17 at the distal tip of the photoreceptor OS promotes cell-autonomous disc shedding.